Article

Discovery Medicine 2026; 38(212): 3016–3027
https://doi.org/10.24976/Discov.Med.202638212.232

XPR1 Promotes the Malignant Phenotypes of Thyroid Carcinoma Cells Partly Through NF-κB-Related Signaling

Jie You[1], Tongxin Zou[1], Boxi Wang[2], Buran Chen[3], Yefeng Cai[1], Renyi Xiao[1], Endong Chen[3], Dixin Xue[4,*], Ming Yu[4,*]

[1]Department of Thyroid Surgery, The First Affiliated Hospital of Wenzhou Medical University, 325000 Wenzhou, Zhejiang, China
[2]Postgraduate Training Base Alliance of Wenzhou Medical University (Zhejiang Provincial People's Hospital), 325000 Wenzhou, Zhejiang, China
[3]Department of Breast Surgery, The First Affiliated Hospital of Wenzhou Medical University, 325000 Wenzhou, Zhejiang, China
[4]Department of Thyroid and Breast Surgery, The Third Affiliated Hospital of Wenzhou Medical University, 325200 Wenzhou, Zhejiang, China
*Correspondence: xuedixin2025@163.com (Dixin Xue); ymszc@126.com (Ming Yu)
Submitted: 23 June 2026 Revised: 5 August 2026 Accepted: 14 August 2026 Published: 23 September 2026

Background: Xenotropic and polytropic retrovirus receptor 1 (XPR1) is highly expressed in human thyroid carcinoma (TC), yet its functional role remains unclear. In this study, we sought to determine whether XPR1 participates in the progression of thyroid carcinoma and to further uncover the molecular pathways associated with its function.

Methods: XPR1 expression in thyroid carcinoma tissues was analyzed using public databases, including Gene Expression Omnibus (GEO), The Cancer Genome Atlas (TCGA), Gene Expression Profiling Interactive Analysis 2 (GEPIA2), and the Human Protein Atlas (HPA). XPR1 expression in thyroid carcinoma cell lines was further validated by quantitative real-time PCR (qRT-PCR) and Western blotting. Following siRNA-mediated silencing of XPR1, cell proliferative activity, clonogenic potential, and migration and invasion abilities were systematically assessed through Cell Counting Kit-8 (CCK-8) assays, clonogenic analyses, and Transwell-based experiments. Apoptotic events and the activation status of nuclear factor kappa-B (NF-κB) signaling were determined through flow cytometric analysis in combination with immunoblotting assays. Rescue experiments were performed by overexpression of p65 cDNA to restore NF-κB signaling activity.

Results: Integrated analyses of GEO, TCGA, GEPIA2, and HPA datasets revealed elevated XPR1 expression in thyroid carcinoma tissues, which was further validated in thyroid carcinoma cell lines by qRT-PCR and Western blotting. Silencing XPR1 markedly suppressed the proliferative capacity, clonogenic growth, migratory and invasive abilities of thyroid carcinoma cells, while simultaneously enhancing apoptotic activity ($p < 0.01$). XPR1 depletion was associated with reduced p65 phosphorylation and altered expression of the apoptosis-related proteins B-cell lymphoma 2 (BCL-2) and Bax ($p < 0.05$). Overexpression of p65 partially reversed these changes and attenuated the inhibitory effects of XPR1 silencing ($p < 0.05$).

Conclusion: Our results suggest that the pro-tumorigenic effects of XPR1 in thyroid carcinoma cells, manifested by increased cell growth, motility, invasiveness, and reduced susceptibility to apoptosis, may be partly associated with NF-κB signaling. Taken together, these findings suggest that XPR1 is involved in the malignant progression of thyroid carcinoma and may represent a potential molecular target worth further investigation.

Keywords: XPR1; thyroid carcinoma; NF-κB signaling; apoptosis

Introduction

Thyroid carcinoma represents one of the most lethal malignancies of the endocrine system. Although most patients achieve favorable outcomes following surgical resection or radioactive iodine therapy, those presenting with local invasion or distant metastases continue to face a substantial risk of recurrence and disease-related mortality [1,2]. A deeper understanding of the molecular events that contribute to thyroid carcinoma progression may facilitate the identification of new therapeutic targets.

Xenotropic and polytropic retrovirus receptor 1 (XPR1) is a membrane-spanning protein composed of 696 amino acid residues. It is an exclusive cell surface receptor for heterophilic and polytropic murine leukemia virus (MLV) [3]. Previous studies indicate that XPR1 participates in the engagement of G proteins and modulates downstream signaling events mediated by G protein–coupled pathways [4,5]. XPR1 has homology with proteins involved in regulating phosphate transport (PHO1, PHO90, and PHO91) [6,7], and has been identified as a key contributor to the regulation of inorganic phosphate export from human cells [8]. It has been reported that stimulation of nu-

clear factor kappa-B (NF-κB) signaling via its receptor in mouse osteoclasts leads to increased XPR1 expression, implying a possible involvement of XPR1 in bone resorption [9]. Several studies have reported that XPR1 acts as the gene underlying brain calcification, highlighting its critical role in this pathological process [10,11]. Nevertheless, the understanding of XPR1's role in cancer progression, both clinically and biologically, remains limited. Previous studies have suggested that XPR1 contributes to the progression of tongue squamous cell carcinoma [12] and has also been reported to be dysregulated in papillary thyroid carcinoma [13]. However, its biological function and the underlying mechanisms in thyroid carcinoma remain incompletely understood.

The NF-κB signaling pathway has been recognized as a central regulator of cellular survival, proliferation, inflammatory responses, and metastatic processes across various cancers [14,15]. Under physiological conditions, NF-κB proteins remain sequestered within the cytoplasmic compartment as a result of their association with inhibitory IκB molecules. Upon stimulation by cytokines, growth factors, or cellular stress, IκBs undergo phosphorylation and subsequent degradation, which permits NF-κB dimers to translocate into the nucleus and initiate transcription of target genes. Enhanced NF-κB signaling in thyroid carcinoma has been associated with tumor progression, including increased proliferation, apoptosis resistance, and greater invasive and metastatic behavior. A previous study has further demonstrated that SPRED3 can upregulate NF-κB signaling to promote thyroid cancer cell proliferation, indicating a mechanistic link between NF-κB activation and tumor growth in TC [16]. Constitutive activation of NF-κB signaling components, including NF-κB-inducing kinase (NIK), has been reported to enhance invasiveness in thyroid carcinoma cell lines, highlighting the involvement of NF-κB pathways in metastatic progression [17]. More recently, synergistic regulation of NF-κB nuclear translocation by deubiquitinases USP14 and UCHL5 has been reported to promote progression in anaplastic thyroid cancer, further linking NF-κB activation with aggressive disease phenotypes [18]. These findings indicate that pathways associated with NF-κB may be critically involved in the progression of thyroid carcinoma.

Nevertheless, although XPR1 has recently been implicated in papillary thyroid carcinoma, its biological role in different thyroid carcinoma cell models and its potential association with NF-κB signaling remain incompletely understood.

Materials and Methods

Bioinformatics

Gene expression datasets associated with thyroid carcinoma were obtained from the publicly accessible Gene Expression Omnibus (GEO) database (https://www.ncbi.nlm.nih.gov/geo/). The microarray datasets GSE33630 and GSE85457, each consisting of thyroid carcinoma specimens alongside matched non-tumorous thyroid samples, were included in the subsequent analyses. Raw transcriptomic data were processed and normalized following established analytical pipelines in the R environment. The identification of differentially expressed genes between thyroid carcinoma tissues and corresponding normal samples was conducted using the limma package in R. *p* values were adjusted for multiple testing using the Benjamini–Hochberg (BH) method to control the false discovery rate (FDR). Genes meeting the criteria of a |log2 fold change| of at least 1, together with an adjusted *p* value (FDR) < 0.05 were defined as DEGs. The overall distribution of DEGs in each dataset was visualized using volcano plots.

The expression profiles of XPR1 across various cancers were analyzed using the "Gene_DE" module available in the TIMER2.0 database (http://timer.cistrome.org). By combining gene expression data from the TCGA database, TIMER2.0 enables the evaluation of XPR1 expression differences by comparing malignant samples with their corresponding non-cancerous counterparts among multiple cancer entities. To evaluate the association between XPR1 expression and immune cell infiltration in thyroid carcinoma, the "Immune-Gene" module of the TIMER2.0 database was used. Immune cell infiltration levels were estimated using the TIMER deconvolution algorithm, and the correlations between XPR1 expression and the abundance of infiltrating immune cells were assessed using Spearman's correlation analysis. Correlation coefficients (R) and corresponding *p* values were obtained directly from the TIMER2.0 platform.

The GEPIA2 web server (http://gepia2.cancer-pku.cn/) was accessed, and the "Expression DIY" module on the homepage was utilized for subsequent analyses. The target gene XPR1 was entered, and thyroid carcinoma (THCA) was chosen as the cancer type. Differential expression analysis of XPR1 was carried out by comparing its expression between thyroid carcinoma tissues and corresponding normal thyroid samples.

Immunohistochemical staining images depicting XPR1 protein levels in thyroid carcinoma specimens and adjacent non-tumorous thyroid tissues were retrieved from the Human Protein Atlas database (HPA) database (https://www.proteinatlas.org/).

Furthermore, the relationship between XPR1 expression and patient survival in thyroid carcinoma (THCA) was evaluated using the GEPIA2 platform. Disease-free survival (DFS) analysis was performed using GEPIA2. Patients were divided into high- and low-expression groups using the median expression value (50% cutoff). Survival curves were generated using the Kaplan–Meier method, and statistical significance was evaluated by the log-rank test. Cases with incomplete survival information were excluded automatically by the GEPIA2 platform.

To further investigate the biological functions and signaling pathways associated with XPR1 in thyroid carcinoma, Gene Set Enrichment Analysis (GSEA) was performed using RNA sequencing data from The Cancer Genome Atlas (TCGA)-THCA cohort. Patients were stratified into high- and low-XPR1 expression groups according to the median expression level of XPR1. GSEA was conducted using GSEA software (version 4.3.2, Broad Institute, Cambridge, MA, USA) with the Hallmark gene set collection (h.all.v2023.1.Hs.symbols.gmt) downloaded from the Molecular Signatures Database (MSigDB). A total of 1000 gene set permutations were performed. Gene sets with a nominal p value < 0.05 and a false discovery rate (FDR) <0.25 were considered significantly enriched.

Cell Lines

TPC-1 (Cat. No. CL-0643), FTC-133 (Cat. No. CL-0644) and BCPAP (Cat. No. CL-0575) were purchased from Procell Life Science & Technology Co., Ltd. (Wuhan, China). The HTORI-3 cell line was purchased from the Shanghai Yaji Biotechnology Co., Ltd (Cat. No. YS4002C). The identity of all cell lines was confirmed using short tandem repeat–based genotyping, and all cultures were verified to be free of mycoplasma contamination. HTORI-3, TPC-1, BCPAP, and FTC-133 cell lines were cultured in RPMI-1640 medium (Cat. No. 11875-093, Gibco, Grand Island, NY, USA) supplemented with 10% fetal bovine serum (FBS, Cat. No. 10099-141, Gibco, Grand Island, NY, USA) and 1% penicillin-streptomycin (Cat. No. 15140-122, Gibco, Grand Island, NY, USA) at 37 °C in a humidified atmosphere containing 5% CO_2.

Cell Transfection

Small interfering RNAs (siRNAs) targeting XPR1 and a non-targeting negative control siRNA (si-NC) were synthesized by GenePharma (Shanghai, China). Cells were transfected with siRNAs at a final concentration of 50 nM (final volume 2 mL per well in 6-well plates) using Lipofectamine RNAiMAX (Cat. No. 13778075, Thermo Fisher Scientific, Waltham, MA, USA) according to the manufacturer's instructions. The XPR1-targeting siRNA sequences were as follows: sense, 5′-GCAUGCUUCUUUGCUCCAATT-3′ and antisense, 5′-UUGGAGCAAAGAAGCAUGCTT-3′. The si-NC sequences were: sense, 5′-UUCUCCGAACGUGUCACGUTT-3′ and antisense, 5′-ACGUGACACGUUCGGAGAATT-3′.

For rescue experiments, cells were co-transfected with si-XPR1 and a p65 overexpression plasmid (OriGene, RC226840) using Lipofectamine 3000 reagent (Cat. No. L3000015, Invitrogen, Carlsbad, CA, USA) [19]. Empty vector plasmids were used as negative controls. The final plasmid concentration used for transfection was 2 µg per well in 6-well plates (final volume 2 mL per well).

Cell Proliferation Assay

Cell proliferation was evaluated using the Cell Counting Kit-8 (CCK-8, Cat. No. C0037, Beyotime Biotechnology, Shanghai, China) according to the manufacturer's protocol. Briefly, 48 h after transfection, cells were harvested and seeded into 96-well plates at a density of 1×10^3 cells per well. At 24 h, 48 h, and 72 h post-seeding, 10 µL of CCK-8 solution was added to each well and incubated at 37 °C for 3 h. Absorbance at 450 nm was subsequently measured using a microplate reader (ELX800, BioTek Instruments, VT, USA).

Clone Formation Experiment

Transfected thyroid carcinoma cells were seeded into 6-well plates at a density of 800 cells per well and cultured under standard conditions for 10–14 days, with the culture medium replaced every 3 days. Colonies were subsequently fixed with 4% paraformaldehyde (Cat. No. P0099, Beyotime, Shanghai, China) at room temperature for 15 min and stained with 0.1% crystal violet (Cat. No. C0121, Beyotime, Shanghai, China). Images of stained colonies were captured using a digital imaging system. Colonies containing more than 50 cells were counted under a light microscope. Quantitative analysis was performed using ImageJ software (National Institutes of Health, Bethesda, MD, USA).

Cell Migration and Invasion Test

Transwell assays based on a 24-well configuration were employed to assess the migration and invasion abilities of cells (8-µm pore size, Cat. No. 34228, Corning, NY, USA). For invasion assays, the upper chamber membranes were coated with Matrigel (Cat. No. 356234, Corning, NY, USA), diluted 1:8 with serum-free RPMI-1640 medium (50 µL per insert) and incubated at 37 °C for 1 h before use, while migration assays used uncoated membranes. Transfected and control thyroid carcinoma cells were detached using 0.25% trypsin (Cat. No. 15090-046, Gibco, Grand Island, NY, USA), resuspended in serum-free RPMI-1640 medium, and 35,000 cells in 200 µL were seeded into the upper chamber. The lower chamber was loaded with 600 µL of RPMI-1640 medium supplemented with 10% FBS to function as a chemoattractant during the migration/invasion assay. After incubation at 37 °C with 5% CO_2 for 24 h, cells remaining on the upper surface of the membrane were carefully removed. Cells that had migrated or invaded to the lower surface were fixed with 4% paraformaldehyde (Cat. No. P0099, Beyotime, Shanghai, China) for 15 min and subsequently stained with 0.1% crystal violet (Cat. No. C0121, Beyotime, Shanghai, China) for visualization. Images from three randomly selected fields on each membrane were captured using an Olympus CKX53 inverted microscope (Olympus, Tokyo, Japan). The numbers of migrated or invaded cells were manually counted using ImageJ software (NIH, Bethesda, MD, USA).

Apoptosis Analysis

Apoptosis was evaluated using the Annexin V-FITC Apoptosis Detection Kit (Cat. No. 556547; Becton, Dickinson and Company, Franklin Lakes, NJ, USA). Forty-eight hours post-transfection, cells were harvested, washed with cold PBS, and stained with Annexin V-FITC and propidium iodide (PI) for 15 min at room temperature in the dark. The stained cells were subsequently analyzed using a BD FACSCanto II flow cytometer (BD Biosciences, Franklin Lakes, NJ, USA). The percentages of early apoptosis (Annexin V^+/PI^-, Q3) and late apoptosis (Annexin V^+/PI^+, Q2) were summed to calculate the total apoptosis rate.

Quantitative Real-Time PCR (qRT-PCR)

Total RNA was isolated from TC cells using TRIzol reagent (Cat. No. 15596026, Thermo Fisher Scientific, Waltham, MA, USA). Complementary DNA (cDNA) was synthesized using the PrimeScript™ RT reagent Kit (Cat. No. RR037A, Takara, Tokyo, Japan). Quantitative real-time PCR (qRT-PCR) was performed using TB Green® Premix Ex Taq™ II (Cat. No. RR820A, Takara, Tokyo, Japan) on an Applied Biosystems 7500 Real-Time PCR System (Applied Biosystems, Thermo Fisher Scientific, Waltham, MA, USA). Relative expression levels of target genes were determined using the $2^{-\Delta\Delta Ct}$ method, with glyceraldehyde-3-phosphate dehydrogenase (GAPDH) employed as the internal reference gene. The primer sequences used for qRT-PCR were as follows: GAPDH, forward: 5′-GTCTCCTCTGACTTCAACAGCG-3′, reverse: 5′-ACCACCCTGTTGCTGTAGCCAA-3′; XPR1, forward: 5′-TGTGTATCCACTTGCCCTTTAT-3′, reverse: 5′-CAGCCAAAACCGGGATTTATAG-3′. NF-κB p65, forward: 5′-TGAACCGAAACTCTGGCAGCTG-3′, reverse: 5′-CATCAGCTTGCGAAAAGGAGCC-3′.

Western Blot

Total protein was isolated from cells using RIPA lysis buffer (Cat. No. P0013B, Beyotime, Shanghai, China), and protein concentrations were quantified with a BCA Protein Assay Kit (Cat. No. P0012, Beyotime, Shanghai, China). Equal amounts of protein were separated by SDS-PAGE and subsequently transferred onto polyvinylidene fluoride membranes (Cat. No. IPVH00010, Millipore, Billerica, MA, USA). The membranes were then blocked with 5% skim milk (Cat. No. P0216; Beyotime Biotechnology) in TBST for 2 h at room temperature. Next, the membranes were incubated overnight at 4 °C with primary antibodies (1:1000) against XPR1 (Cat. No. ab325878), β-actin (Cat. No. ab8227), P65 (Cat. No. ab32536), phospho-P65 (Ser536) (Cat. No. ab86299), BCL-2 (Cat. No. ab32124), and Bax (Cat. No. ab32503) (Abcam, Cambridge, MA, USA). Following TBST washes, the membranes were incubated with HRP-conjugated secondary antibodies (Cat. No. ab6721 and Cat. No. ab6728, Abcam, Cambridge, MA, USA) for 1 h at room temperature. Protein bands were then detected using an enhanced chemiluminescence (ECL) detection kit (Cat. No. P0018S, Beyotime, Shanghai, China). Band intensities were quantified using ImageJ software and normalized to β-actin or p65.

Statistical Analysis

Statistical analyses were conducted using SPSS version 23.0 (IBM, Armonk, NY, USA), and graphical representations were created with GraphPad Prism 8 (GraphPad Software, La Jolla, CA, USA). Data are expressed as the mean ± standard deviation (SD) from at least three independent experiments. Normality of the data distribution was assessed using the Shapiro–Wilk test prior to parametric analysis. Differences between two groups were evaluated using the Student's *t*-test, whereas comparisons among multiple groups were analyzed by one-way analysis of variance (ANOVA) followed by Tukey's post hoc test. A *p*-value of less than 0.05 was considered statistically significant.

Results

XPR1 Is Significantly Upregulated in TC

Transcriptomic analyses of the GSE33630 and GSE85457 datasets identified DEGs between TC and normal tissues, as visualized by volcano plots (Fig. 1A). Intersection analysis of the two datasets revealed that XPR1 was among the consistently upregulated genes in TC (Fig. 1B). Pan-cancer analysis using the TCGA dataset showed that XPR1 was differentially expressed across multiple cancer types, including thyroid carcinoma (Fig. 1C). Further analysis of the TCGA THCA cohort demonstrated that XPR1 mRNA expression was significantly higher in thyroid carcinoma tissues than in non-tumorous thyroid tissues ($p < 0.05$, Fig. 1D). Protein-level validation using HPA IHC images demonstrated stronger XPR1 staining in TC tissues relative to normal tissues (Fig. 1E). Moreover, GEPIA2-based analyses revealed a significant correlation between higher XPR1 expression levels and disease-free survival outcomes among individuals with thyroid carcinoma, underscoring the possible prognostic value of XPR1 ($p < 0.05$, Fig. 1F). Using the TIMER platform, we further examined the association between XPR1 expression and immune cell infiltration, revealing positive correlations with B cells, $CD4^+$ T cells, macrophages, neutrophils, and dendritic cells ($p < 0.05$, Fig. 1G). Taken together, these findings demonstrate that XPR1 expression is markedly elevated in thyroid carcinoma and correlates with immune cell infiltration, suggesting a potential role in tumor progression and modulation of the tumor immune microenvironment.

XPR1 Knockdown Inhibits Proliferation, Migration, and Invasion of TC Cells

We initially evaluated XPR1 expression in thyroid carcinoma cell lines (TPC-1, BCPAP, FTC-133) and normal

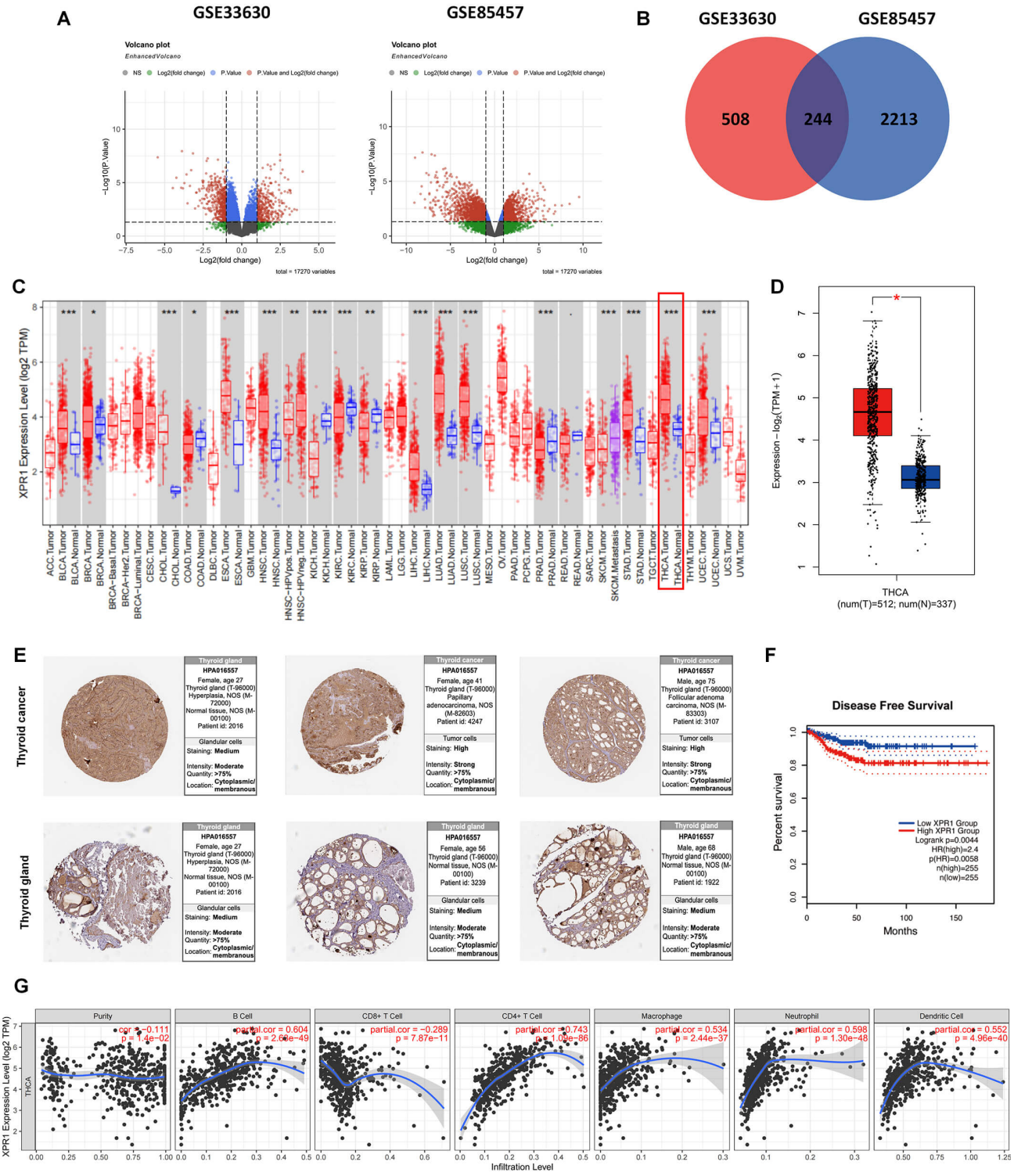

Fig. 1. XPR1 expression analysis in TC. (A) Volcano plots of DEGs in GSE33630 and GSE85457. (B) Intersection of DEGs from the two GEO datasets. (C) Pan-cancer analysis of XPR1 expression using TCGA datasets. (D) XPR1 mRNA expression in TCGA THCA tumor and normal tissues. (E) IHC images of XPR1 from HPA. (F) DFS analysis based on XPR1 using GEPIA2. (G) Correlation between XPR1 and immune infiltration analyzed with TIMER. *$p < 0.05$, **$p < 0.01$, ***$p < 0.001$. XPR1, xenotropic and polytropic retrovirus receptor 1; TC, thyroid carcinoma; DEGs, differentially expressed genes; TCGA, The Cancer Genome Atlas; IHC, immunohistochemistry; HPA, Human Protein Atlas.

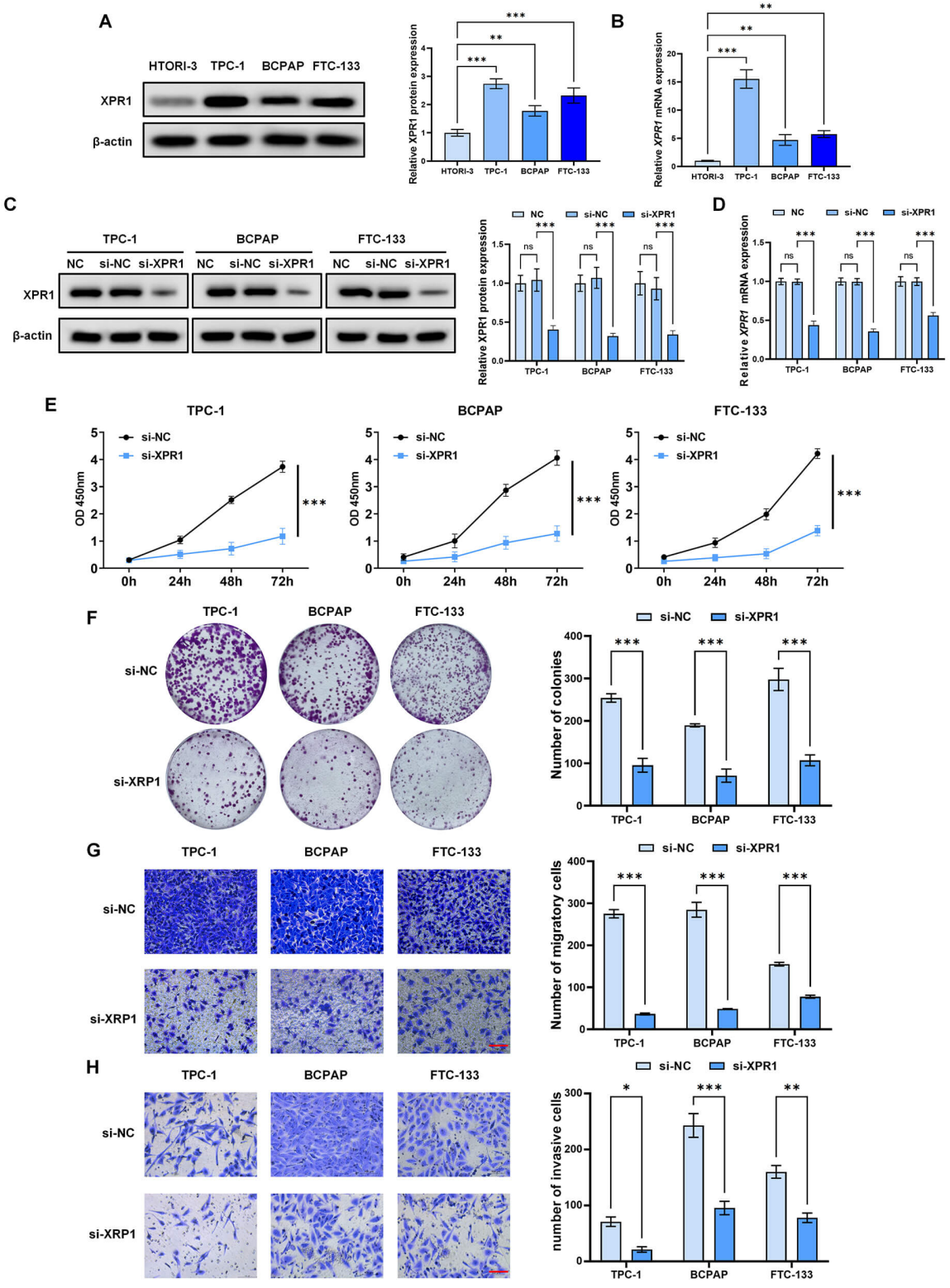

Fig. 2. XPR1 expression and functional analysis in TC cells. (A) XPR1 protein levels in the four cell lines detected by WB. (B) XPR1 mRNA levels in HTORI-3, TPC-1, BCPAP, and FTC-133 cells measured by qRT-PCR. (C,D) XPR1 protein and mRNA levels in TPC-1, BCPAP, and FTC-133cells after siRNA-mediated knockdown. (E) Cell proliferation assessed by CCK-8 assay. (F) Colony formation assay. (G) Transwell migration assay. (H) Transwell invasion assay. Scale bar = 100 μm. Data are shown as mean ± SD, (n = 3). *p <0.05, **p < 0.01, ***p < 0.001; ns, not significant.

thyroid cells (HTORI-3) at both the protein and mRNA levels. Compared with HTORI-3 cells, XPR1 expression was substantially elevated in all three TC cell lines ($p < 0.01$, Fig. 2A,B). To investigate the functional role of XPR1, we silenced its expression using si-XPR1 in TPC-1, BCPAP, and FTC-133 cells, which effectively reduced XPR1 protein and mRNA levels ($p < 0.001$, Fig. 2C,D). CCK-8–based measurements were employed to assess changes in proliferative capacity following XPR1 silencing, revealing a marked reduction in growth across all three thyroid carcinoma cell lines (Fig. 2E). Similarly, colony formation assays confirmed that XPR1 depletion suppressed the clonogenic ability of TC cells ($p < 0.001$, Fig. 2F). Furthermore, Transwell assays demonstrated that silencing XPR1 reduced the number of migrated and invaded TC cells ($p < 0.001$, Fig. 2G,H). Taken together, the data reveal elevated XPR1 levels in thyroid carcinoma cells, while its silencing significantly suppresses cellular proliferation, migration, and invasive behavior.

XPR1 Knockdown Promotes Apoptosis and Is Associated With Reduced p65 Phosphorylation in TC Cells

To elucidate the potential biological functions associated with XPR1 in thyroid cancer, TCGA-THCA data were subjected to single-gene–driven GSEA after categorizing samples into XPR1-high and XPR1-low groups. GSEA revealed that apoptosis-related and NF-κB signaling–related gene sets were significantly associated with XPR1 expression in TC (Fig. 3A,B). We then assessed apoptosis in TPC-1, BCPAP, and FTC-133 cells following siRNA-mediated XPR1 knockdown. Flow cytometry showed increased apoptosis in all three cell lines ($p < 0.01$, Fig. 3C). Western blot analysis demonstrated that XPR1 depletion reduced the p-p65/p65 ratio, decreased BCL-2, and increased Bax levels ($p < 0.001$, Fig. 3D), suggesting reduced p65 phosphorylation and potential attenuation of NF-κB signaling activity. These findings suggest that silencing XPR1 enhances programmed cell death while being accompanied by reduced p65 phosphorylation and changes in apoptosis-related proteins that are consistent with altered NF-κB signaling in thyroid carcinoma cells.

NF-κB Activation Rescues the Effects of XPR1 Knockdown in TC Cells

To further investigate the involvement of the NF-κB signaling pathway in thyroid cancer, TPC-1 and BCPAP cells were selected for p65 overexpression experiments due to their stable growth characteristics and high transfection efficiency. To verify the effectiveness of p65 overexpression prior to subsequent functional rescue assays, cells were transfected with either the p65 cDNA overexpression plasmid or the corresponding empty vector. Western blot analysis demonstrated that p65 protein expression was markedly elevated in both TPC-1 and BCPAP cells following p65 cDNA transfection compared with the Vector group ($p < 0.001$, Fig. 4A). Consistently, qRT-PCR analysis confirmed a significant increase in *p65* mRNA expression in the p65 cDNA group ($p < 0.001$, Fig. 4B), indicating successful establishment of the p65 overexpression model for subsequent mechanistic experiments.

Subsequently, rescue experiments were performed in TPC-1 and BCPAP cells, which were divided into three groups: si-NC, si-XPR1, and si-XPR1 + p65 cDNA overexpression. Multiple *in vitro* assays were then conducted to evaluate cellular proliferative capacity, clonogenic ability, as well as migratory and invasive behaviors. CCK-8 analysis demonstrated that silencing XPR1 markedly inhibited cell growth, while stimulation with p65 cDNA overexpression partially reversed the proliferation-suppressive effect ($p < 0.001$, Fig. 4C). Similarly, colony formation assays demonstrated that XPR1 silencing reduced clonogenic capacity, which was rescued by p65 cDNA overexpression ($p < 0.001$, Fig. 4D). Transwell assays demonstrated that XPR1 knockdown significantly decreased the number of migrated and invaded TPC-1 and BCPAP cells ($p < 0.001$, Fig. 4E,F), whereas NF-κB activation partially reversed these inhibitory effects. Taken together, the results indicate that silencing XPR1 suppresses proliferation, colony-forming ability, motility, and invasiveness partly in association with changes in NF-κB signaling.

NF-κB Activation Rescues XPR1 Knockdown-Induced Apoptosis in TC Cells

Flow cytometry analysis demonstrated that XPR1 knockdown markedly enhanced apoptosis in both TPC-1 and BCPAP cells relative to the si-NC control, whereas p65 cDNA overexpression partially reversed the pro-apoptotic effect of si-XPR1 ($p < 0.01$, Fig. 5A). Western blot analysis showed that si-XPR1 reduced the p-p65/p65 ratio and BCL-2 expression while increasing Bax levels, indicating activation of apoptotic signaling in TPC-1 and BCPAP cells. Notably, p65 cDNA overexpression partially restored p-p65 and BCL-2 levels and decreased Bax, corresponding with a partial rescue of apoptosis, suggesting partial restoration of p65 phosphorylation and NF-κB–related signaling changes ($p < 0.001$, Fig. 5B). Overall, the data suggest that NF-κB activation can partly mitigate the apoptosis induced by XPR1 silencing, suggesting that the effects of XPR1 on apoptosis may be partly associated with NF-κB signaling in thyroid carcinoma cells.

Discussion

Thyroid cancer represents the most prevalent endocrine malignancy, occurring more frequently in women and ranking fifth in overall incidence [20]. Although patients with thyroid cancer generally exhibit a favorable prognosis, a subset of individuals remains at risk of recurrence or mortality. Therefore, there is a need to identify novel biomarkers and therapeutic targets.

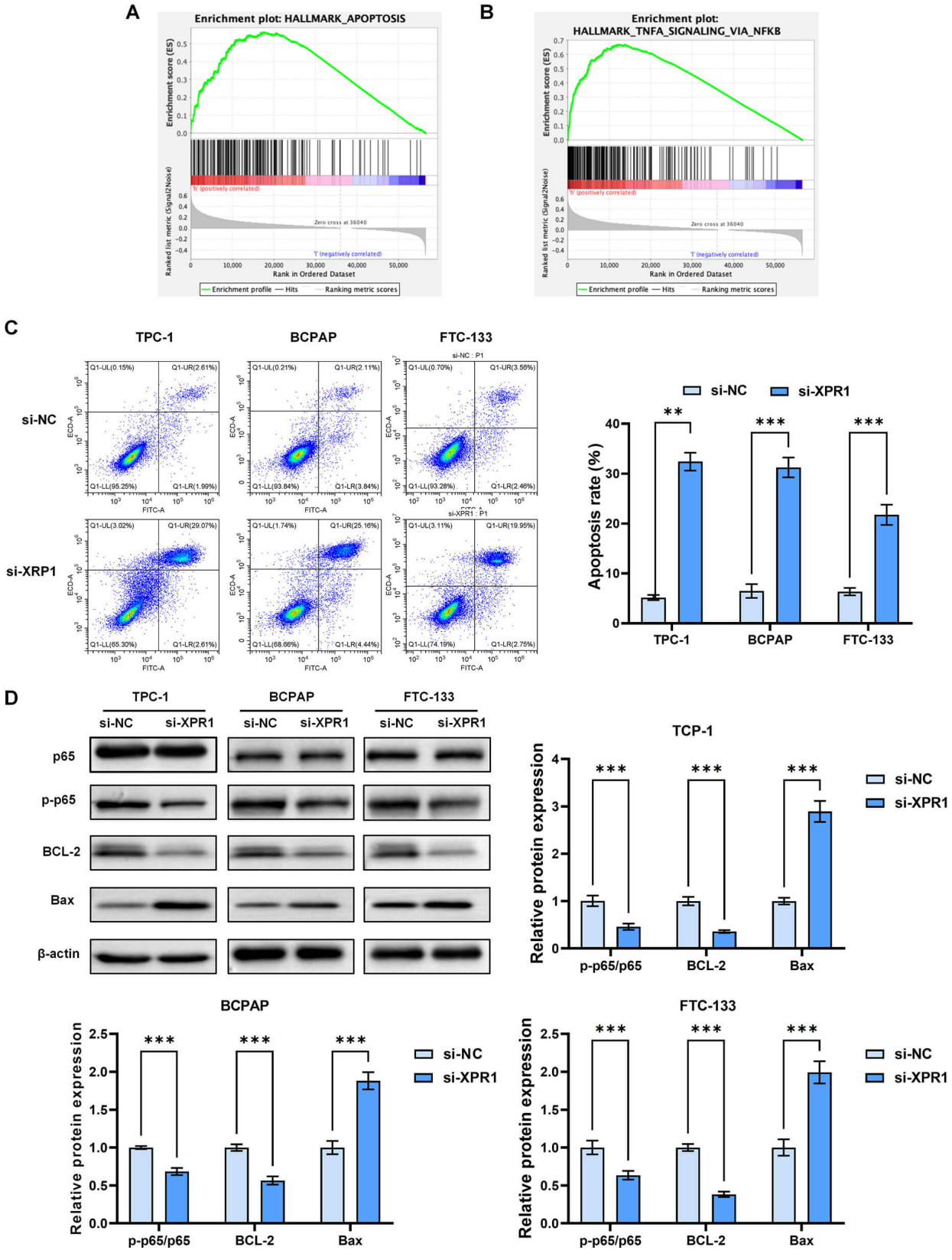

Fig. 3. XPR1 knockdown promotes apoptosis and is associated with reduced p65 phosphorylation in TC cells. (A,B) GSEA of apoptosis- and NF-κB-related genes in high- versus low-XPR1 expression groups from TCGA THCA. (C) Apoptosis analysis in TPC-1, BCPAP, and FTC-133 cells measured by flow cytometry. (D) WB detection of p-p65/p65, BCL-2, and Bax in the three cell lines. Data are shown as mean ± SD, (n = 3). $^{**}p < 0.01$, $^{***}p < 0.001$.

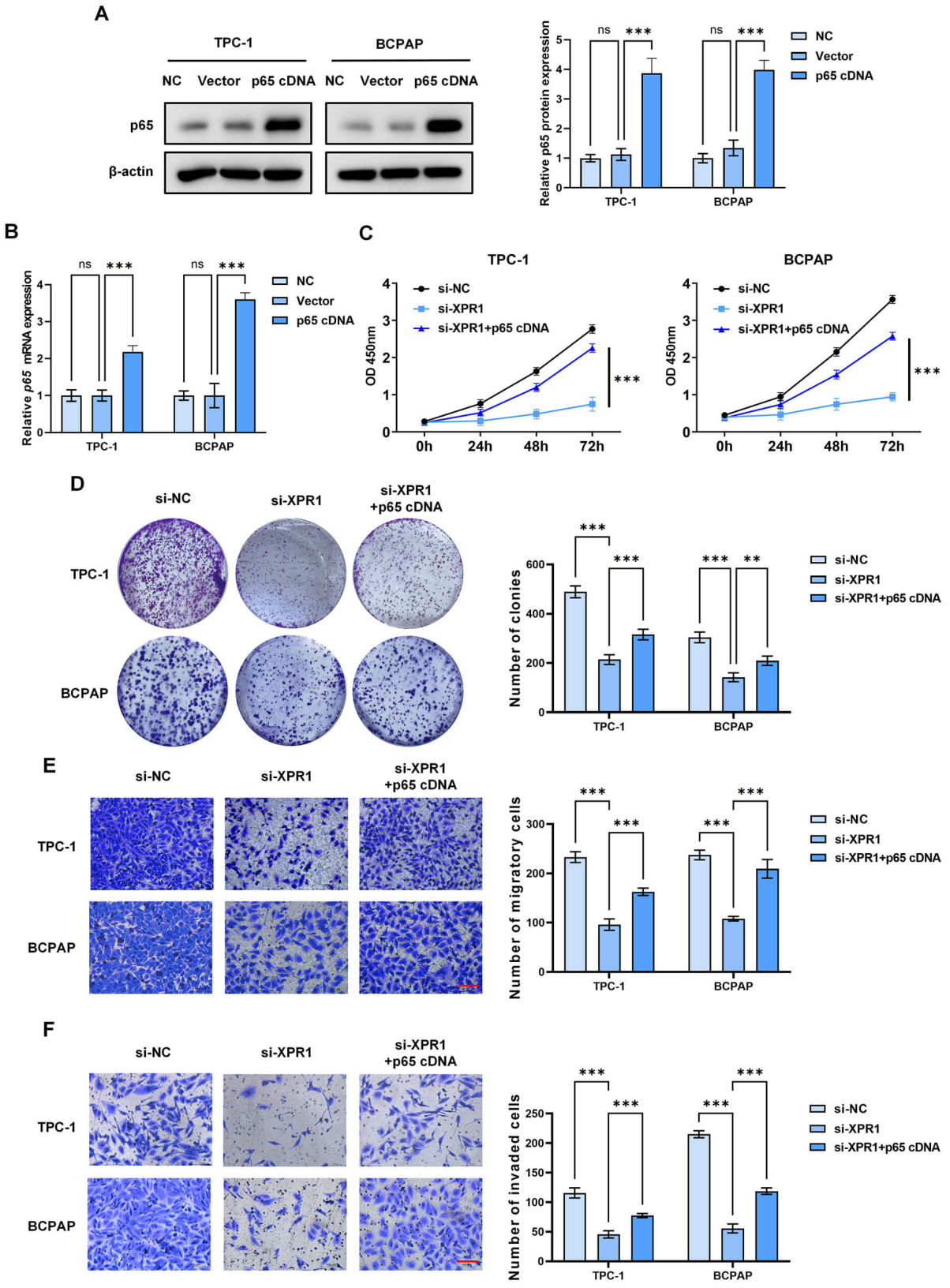

Fig. 4. p65 cDNA overexpression rescues the effects of XPR1 knockdown in TC cells. (A) WB analysis of p65 protein levels in TPC-1 and BCPAP cells across Vector and p65 cDNA groups. (B) qRT-PCR detection of *p65* mRNA. (C) Cell proliferation assessed by CCK-8 assay. (D) Colony formation assay. (E) Transwell migration assay. (F) Transwell invasion assay. Scale bar = 100 μm. Data are shown as mean ± SD, (n = 3). $^{**}p < 0.01$, $^{***}p < 0.001$.

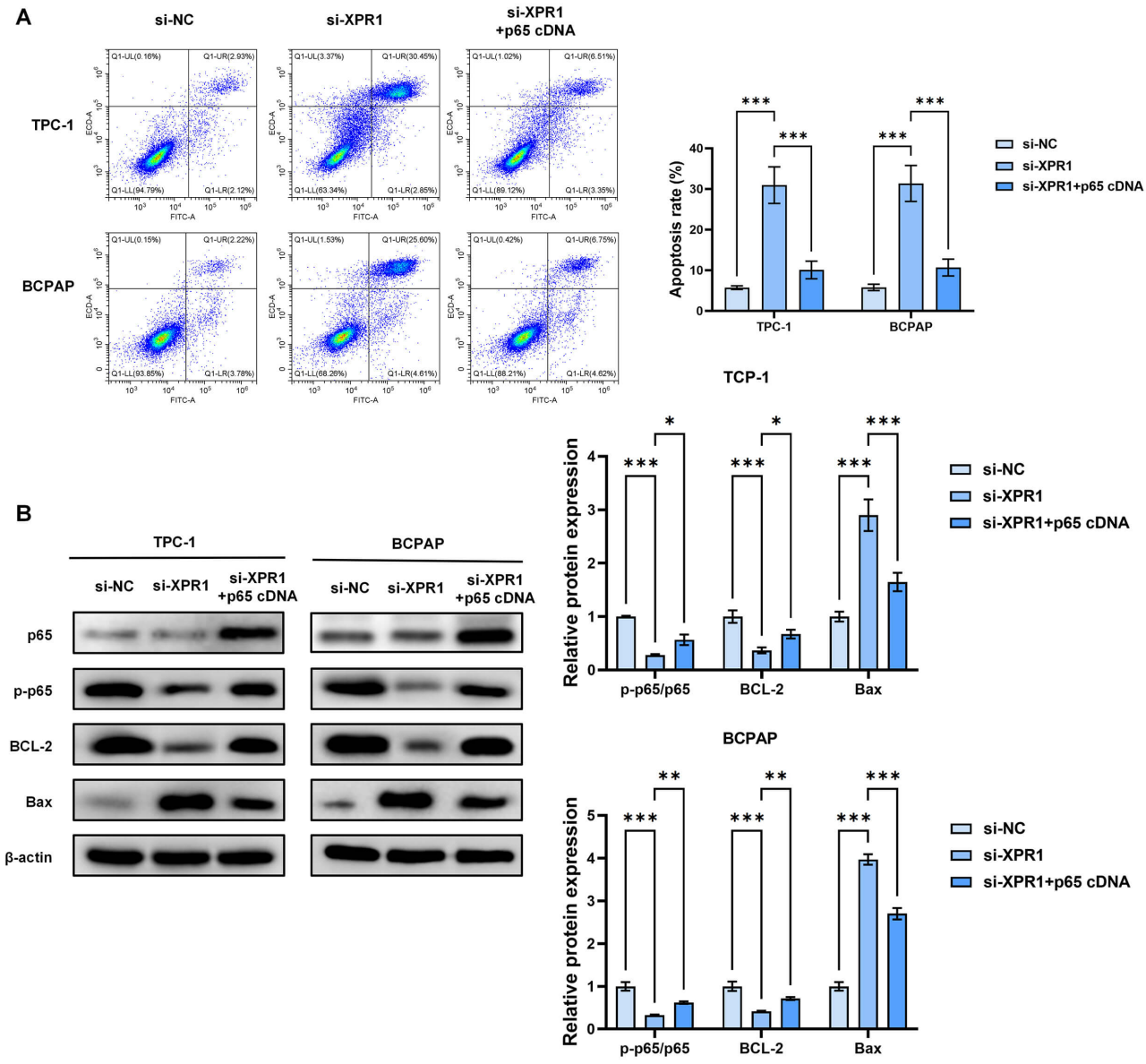

Fig. 5. p65 cDNA overexpression rescues XPR1 knockdown-induced apoptosis in TC cells. (A) Apoptosis of TPC-1 and BCPAP cells assessed by flow cytometry. (B) Western blot analysis of p-p65/p65, BCL-2, and Bax. Data are shown as mean ± SD, (n = 3). *p < 0.05, **p < 0.01, ***p < 0.001.

Identified as a membrane-associated receptor, XPR1 recognizes and facilitates infection by both xenotropic and polytropic forms of murine leukemia virus [21]. Earlier research reported elevated XPR1 levels in tongue and esophageal squamous cell carcinomas, where it enhances cancer cell proliferation and migratory capacity [22,23]. Given its established pro-tumorigenic roles in multiple epithelial malignancies, the contribution of XPR1 to thyroid cancer progression warrants further investigation.

In this study, transcriptomic analyses of the GSE33630 and GSE85457 datasets identified XPR1 as one of the consistently upregulated genes in TC. XPR1 is significantly upregulated in thyroid carcinoma cells and is associated with immune cell infiltration, implicating its role in tumor progression and the immune microenvironment in TC. Functional experiments in thyroid carcinoma cell lines further demonstrated that silencing XPR1 markedly reduced proliferative activity, colony-forming potential, migratory behavior, and invasive capacity. Previous research has indicated that XPR1 is markedly overexpressed in papillary thyroid carcinoma cells, promoting tumor cell growth, motility, and invasiveness via oncogenic signaling pathways. However, these previous studies mainly focused on papillary thyroid carcinoma cells, whereas the present study included both papillary (TPC-1 and BCPAP) and follicular (FTC-133) thyroid

carcinoma cell lines in the loss-of-function experiments to further evaluate the biological effects of XPR1 across different thyroid carcinoma cell backgrounds. Higher XPR1 levels have also been correlated with shorter disease-free survival among patients [13]. Moreover, in hepatocellular carcinoma models, increased XPR1 expression was linked to poor prognosis, and its knockdown induced mitochondrial dysfunction and apoptosis, indicating a wider role for XPR1 in supporting cancer cell survival and progression [24].

Single-gene GSEA and Western blot analyses revealed that XPR1 knockdown suppressed NF-κB signaling and modulated apoptosis-related proteins, including BCL-2 and Bax. Rescue experiments with p65 cDNA overexpression confirmed that NF-κB activation partially reversed the effects of XPR1 depletion, suggesting that the biological effects of XPR1 may be partly associated with NF-κB signaling. In other cancer types, such as tongue squamous cell carcinoma, XPR1 overexpression enhanced malignant phenotypes and activated NF-κB signaling, whereas its silencing inhibited proliferation, invasion, and anti-apoptotic capacity, indicating that XPR1-mediated NF-κB activation contributes to tumor progression [22]. Emerging studies have also highlighted the central role of NF-κB as a regulator of cancer cell survival and cell death pathways. A recent comprehensive review and analysis indicated that NF-κB activation supports tumorigenesis by promoting proliferation and suppressing programmed cell death, whereas inhibition of NF-κB enhances cancer cell susceptibility to apoptosis [25]. Collectively, these findings support a possible association between XPR1 expression and NF-κB-related signaling changes during thyroid carcinoma cells progression.

Despite our findings, this study has several limitations. First, most functional assays were performed *in vitro*, and *in vivo* validation of XPR1's role in thyroid cancer progression is still lacking. Second, although our results suggest an association between XPR1 expression and changes in NF-κB–related signaling, the molecular mechanism linking the membrane-associated phosphate exporter XPR1 to NF-κB activation, particularly the regulation of p65 phosphorylation, remains unclear. The precise molecular interactions and upstream regulators involved also require further investigation. Third, the clinical relevance of XPR1 expression, including its predictive value for patient response to therapy, requires validation in larger, independent cohorts. Future investigations into these issues are crucial for comprehensively elucidating the therapeutic value of targeting XPR1 in thyroid carcinoma cells. Finally, although loss-of-function experiments were performed in both papillary and follicular thyroid carcinoma cell lines, the rescue experiments were conducted only in the papillary thyroid carcinoma cell lines (TPC-1 and BCPAP). Therefore, the mechanistic findings should be interpreted cautiously and may not be directly generalizable to all histological subtypes of thyroid carcinoma. Future studies should further validate these observations in additional thyroid carcinoma models.

Conclusion

XPR1 is highly expressed in thyroid carcinoma cells and is associated with enhanced malignant phenotypes in thyroid carcinoma cells by enhancing cell growth, motility, and invasiveness, while concurrently reducing apoptosis which may be partly associated with alterations in NF-κB signaling. In addition, XPR1 expression shows a close correlation with patterns of immune cell infiltration, implying its involvement in modulation of the tumor microenvironment. Overall, these findings provide preliminary evidence supporting XPR1 as a potential biomarker and therapeutic target for thyroid carcinoma, although further mechanistic and *in vivo* studies are required.

Availability of Data and Materials

The datasets used or analyzed during the current study are available from the corresponding authors on reasonable request.

Author Contributions

JY and TXZ designed the study and contributed to conceptualization and methodology. BXW, BRC, YFC, and RYX conducted data collection, investigation, validation, and visualization. EDC performed formal analysis and provided technical and software support. DXX and MY contributed to the conception and design of the study, supervised the study, provided resources, and contributed to project administration. JY drafted the original manuscript and all authors contributed to the critical revision of the manuscript for important intellectual content. All authors have read and approved the final manuscript and agreed to be accountable for all aspects of the work.

Ethics Approval and Consent to Participate

Not applicable.

Acknowledgment

Not applicable.

Funding

This work was supported by the Wenzhou Basic Scientific Research Project (Grant No. Y2023156).

Conflict of Interest

The authors declare no conflict of interest.

References

[1] Chen DW, Carr G, Worden FP, Veenstra CM, Haymart MR, Banerjee M. Survival Prognostication in Patients with Differentiated Thyroid Cancer and Distant Metastases: A SEER Population-Based Study. Thyroid : Official Journal of the American Thyroid Association. 2024; 34: 837–845. https://doi.org/10.1089/thy.2023.0709

[2] Khandelwal Y, Satapathy S, Bal C. Brain Metastases in Differentiated Thyroid Carcinoma: Clinical Features, Treatment Outcomes, and the Role of Radioiodine Therapy. Clinical Endocrinology. 2026; 105: 245–251. https://doi.org/10.1111/cen.70142

[3] Yan R, Chen H, Liu C, Zhao J, Wu D, Jiang J, et al. Human XPR1 structures reveal phosphate export mechanism. Nature. 2024; 633: 960–967. https://doi.org/10.1038/s41586-024-07852-9

[4] Spain BH, Koo D, Ramakrishnan M, Dzudzor B, Colicelli J. Truncated forms of a novel yeast protein suppress the lethality of a G protein alpha subunit deficiency by interacting with the beta subunit. The Journal of Biological Chemistry. 1995; 270: 25435–25444. https://doi.org/10.1074/jbc.270.43.25435

[5] Vaughan AE, Mendoza R, Aranda R, Battini JL, Miller AD. Xpr1 is an atypical G-protein-coupled receptor that mediates xenotropic and polytropic murine retrovirus neurotoxicity. Journal of Virology. 2012; 86: 1661–1669. https://doi.org/10.1128/JVI.06073-11

[6] Stefanovic A, Arpat AB, Bligny R, Gout E, Vidoudez C, Bensimon M, et al. Over-expression of PHO1 in Arabidopsis leaves reveals its role in mediating phosphate efflux. The Plant Journal : for Cell and Molecular Biology. 2011; 66: 689–699. https://doi.org/10.1111/j.1365-313X.2011.04532.x

[7] Hürlimann HC, Pinson B, Stadler-Waibel M, Zeeman SC, Freimoser FM. The SPX domain of the yeast low-affinity phosphate transporter Pho90 regulates transport activity. EMBO Reports. 2009; 10: 1003–1008. https://doi.org/10.1038/embor.2009.105

[8] Zhu Q, Yaggi MF, Jork N, Jessen HJ, Diver MM. Transport and $InsP_8$ gating mechanisms of the human inorganic phosphate exporter XPR1. Nature Communications. 2025; 16: 2770. https://doi.org/10.1038/s41467-025-58076-y

[9] Sharma P, Patntirapong S, Hann S, Hauschka PV. RANKL-RANK signaling regulates expression of xenotropic and polytropic virus receptor (XPR1) in osteoclasts. Biochemical and Biophysical Research Communications. 2010; 399: 129–132. https://doi.org/10.1016/j.bbrc.2010.07.022

[10] Yao XP, Zhao M, Wang C, Guo XX, Su HZ, Dong EL, et al. Analysis of gene expression and functional characterization of XPR1: a pathogenic gene for primary familial brain calcification. Cell and Tissue Research. 2017; 370: 267–273. https://doi.org/10.1007/s00441-017-2663-3

[11] Lin Z, Yang D, Wang L, Li J, Chen X, Jin N, et al. The Genetic and Phenotypic Spectrum of Primary Brain Calcification in a Large Cohort from China. Movement Disorders : Official Journal of the Movement Disorder Society. 2025; 40: 1661–1668. https://doi.org/10.1002/mds.30207

[12] Wang L. Bioinformatics analyses proposed xenotropic and polytropic retrovirus receptor 1 as a potential diagnostic and prognostic biomarker and immunotherapeutic target in head and neck squamous cell carcinoma. Auris, Nasus, Larynx. 2023; 50: 134–150. https://doi.org/10.1016/j.anl.2022.05.018

[13] Su Y, Mei L, Wu Y, Li C, Jiang T, Zhao Y, et al. Xenotropic and polytropic retrovirus receptor 1 (XPR1) promotes progression of papillary thyroid carcinoma via the BRAF-ERK1/2-P53 signaling pathway. Journal of Endocrinological Investigation. 2025; 48: 633–652. https://doi.org/10.1007/s40618-024-02481-5

[14] Li J, Cai Q, Wang Z, Wang L, Yang G, Zhang Z, et al. Epithelial-Mesenchymal Transformation Promotes the Progression of Hepatocellular Carcinoma through NF-κB/MMP9 Axis. Discovery Medicine. 2024; 36: 666–677. https://doi.org/10.24976/Discov.Med.202436183.63

[15] Tao J, Wang L, Gu Z, Zhang L. Effect of Bortezomib Treatment in Multiple Myeloma on Blood Coagulation Function, Renal Function, Immune Function, and the NF-κB Pathway-Associated Indicators. British Journal of Hospital Medicine. 2025; 86: 1–15. https://doi.org/10.12968/hmed.2024.0701

[16] Chen Z, Wang C, Li M, Cai S, Liu X. SPRED3 regulates the NF-κB signaling pathway in thyroid cancer and promotes the proliferation. Scientific Reports. 2024; 14: 20506. https://doi.org/10.1038/s41598-024-61075-6

[17] Cormier F, Housni S, Dumont F, Villard M, Cochand-Priollet B, Mercier-Nomé F, et al. NF-κB signaling activation and roles in thyroid cancers: implication of MAP3K14/NIK. Oncogenesis. 2023; 12: 55. https://doi.org/10.1038/s41389-023-00496-w

[18] Zhang S, Han B, Jiang B, Chen M, Mu D, Wang Q, et al. USP14 and UCHL5 synergistically deubiquitinate PKCα and translocate NF-κB to promote the progression of anaplastic thyroid cancer. Cell Death & Disease. 2025; 16: 617. https://doi.org/10.1038/s41419-025-07890-9

[19] You Q, Huang T, He Z, Tao X, Zhang Y, Zhang H, et al. *GJB2* enhances cancer stem cell properties by modulating *SOX2* expression via NF-κB pathway activation in lung adenocarcinoma. Translational Cancer Research. 2025; 14: 2648–2660. https://doi.org/10.21037/tcr-24-2075

[20] Ferlay J, Colombet M, Soerjomataram I, Parkin DM, Piñeros M, Znaor A, et al. Cancer statistics for the year 2020: An overview. International Journal of Cancer. 2021; 149: 778–789. https://doi.org/10.1002/ijc.33588

[21] Chen L, He J, Wang M, She J. Structure and function of human XPR1 in phosphate export. Nature Communications. 2025; 16: 2983. https://doi.org/10.1038/s41467-025-58195-6

[22] Chen WC, Li QL, Pan Q, Zhang HY, Fu XY, Yao F, et al. Xenotropic and polytropic retrovirus receptor 1 (XPR1) promotes progression of tongue squamous cell carcinoma (TSCC) via activation of NF-κB signaling. Journal of Experimental & Clinical Cancer Research : CR. 2019; 38: 167. https://doi.org/10.1186/s13046-019-1155-6

[23] Wu W, Zhang Y, Li X, Wang X, Yuan Y. miR-375 Inhibits the Proliferation, Migration and Invasion of Esophageal Squamous Cell Carcinoma by Targeting XPR1. Current Gene Therapy. 2021; 21: 290–298. https://doi.org/10.2174/1566523220666201229155833

[24] Liao ZQ, Lv YF, Kang MD, Ji YL, Liu Y, Wang LR, et al. Inhibition of XPR1-dependent phosphate efflux induces mitochondrial dysfunction: A potential molecular target therapy for hepatocellular carcinoma? Molecular Carcinogenesis. 2024; 63: 2332–2345. https://doi.org/10.1002/mc.23812

[25] Wu X, Sun L, Xu F. NF-κB in Cell Deaths, Therapeutic Resistance and Nanotherapy of Tumors: Recent Advances. Pharmaceuticals (Basel, Switzerland). 2023; 16: 783. https://doi.org/10.3390/ph16060783